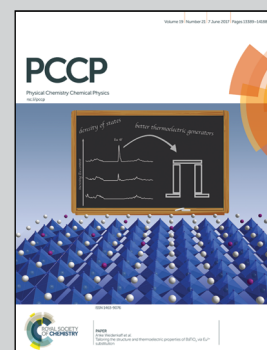


Showcasing research led by Prof. Daniel Strasser at the Institute of Chemistry, Hebrew University of Jerusalem, Israel.

Single-photon Coulomb explosion of methanol using broad bandwidth ultrafast EUV pulses

Towards time resolved probing of molecular dynamics by single-photon Coulomb explosion imaging, we investigated Coulomb explosion of methanol by ultrafast EUV pulses achieved through high-order harmonics generation. *Ab initio* calculations, performed by the group of Prof. Roi Baer, support instantaneous double-ionization and prompt dissociation of the C–O bond on excited dication states. Furthermore, a simple model is presented for relating 3D coincidence imaging data to distances within the neutral molecule geometry.

As featured in:



See Daniel Strasser et al.,  
*Phys. Chem. Chem. Phys.*,  
2017, 19, 13488.



rsc.li/pccp

Registered charity number: 207890



Cite this: *Phys. Chem. Chem. Phys.*,  
2017, **19**, 13488

# Single-photon Coulomb explosion of methanol using broad bandwidth ultrafast EUV pulses

Itamar Luzon,<sup>a</sup> Krishna Jagtap,<sup>a</sup> Ester Livshits,<sup>b</sup> Oleg Lioubashevski,<sup>a</sup> Roi Baer<sup>b</sup> and Daniel Strasser<sup>ib</sup>\*<sup>a</sup>

Single-photon Coulomb explosion of methanol is instigated using the broad bandwidth pulse achieved through high-order harmonics generation. Using 3D coincidence fragment imaging of one molecule at a time, the kinetic energy release (KER) and angular distributions of the products are measured in different Coulomb explosion (CE) channels. Two-body CE channels breaking either the C–O or the C–H bonds are described as well as a proton migration channel forming  $\text{H}_2\text{O}^+$ , which is shown to exhibit higher KER. The results are compared to intense-field Coulomb explosion measurements in the literature. The interpretation of broad bandwidth single-photon CE data is discussed and supported by *ab initio* calculations of the predominant C–O bond breaking CE channel. We discuss the importance of these findings for achieving time resolved imaging of ultrafast dynamics.

Received 26th January 2017,  
Accepted 10th April 2017

DOI: 10.1039/c7cp00587c

rsc.li/pccp

## Introduction

The making of molecular movies, visualizing ultrafast bond rearrangement during chemical reactions, has become a realizable venture with the advent of ultrafast lasers on the femto-second (fs) time scale.<sup>1–3</sup> One of the exciting prospects is the Coulomb explosion (CE) of a molecule into correlated cationic fragments following the sudden stripping of electrons. Coulomb explosion imaging (CEI) has been induced through thin-foil stripping of accelerated molecular ions<sup>4–6</sup> or by inducing multiple ionization in isolated neutral molecules by an intense fs laser pulse.<sup>7–9</sup> In both cases the coincidence imaging of the CE products allowed visualization of the parent molecular structure. However, unlike the thin foil CEI technique, the intense field CE based on ultrafast amplified laser pulses allowed pump probe measurements with femtosecond time resolution. This was used to resolve the controversial double proton transfer in 7-azaindole dimer model for DNA base pairs, inferring sequential proton transfer from protonated monomers in the transient CE product spectrum.<sup>10–12</sup> However, due to the inherent step-wise nature of multi-photon ionization, it was difficult to conclude if the observed proton transfer occurs before the CE, or on an intermediate singly ionized state.<sup>13,14</sup>

Intense field CE work was demonstrated to exhibit fascinating intense field effects, even when full stripping of a simple molecule such as  $\text{H}_2$  is achieved, masking the underlying

structural information.<sup>15–17</sup> In simple molecules such as methanol, proton migration dynamics during intense field CE and its dependence on laser pulse parameters were extensively explored by Yamanouchi and coworkers.<sup>18–20</sup> All intense field CE measurements including proton migration fraction, molecular alignment and KER were demonstrated to strongly depend on laser pulse duration, peak intensity and spectral chirp.<sup>18,19</sup> With decreasing laser pulse durations, the measured KER typically tend to increase towards an asymptotic instantaneous CE limit. Nevertheless, interpretation of intense field CE measurements in terms of molecular structure is generally affected by intense field effects, and therefore difficult to discern.

An alternative path for achieving CE at low field conditions uses a single photon with sufficiently high energy to remove more than one electron.<sup>21–23</sup> X-ray induced Auger decay lead to efficient double ionization following an ejection of a core electron. Nevertheless, also extreme ultraviolet (EUV) photons can induce relatively rare double ionization events.<sup>22,24–27</sup> Based on numerous single photon double ionization experiments, using continuous narrow bandwidth radiation sources, Eland *et al.* developed an empiric law that relates the threshold photon energy to the first ionization potential (IP) and the dication inter-charge distance ( $R$ ):  $h\nu \geq 2.2\text{IP} + 1/(4\pi\epsilon R)$ .<sup>25</sup> Interestingly, the empiric study of Eland and co-workers indicates that the best fitted effective permittivity  $\epsilon$  is 1.25 times higher than vacuum permittivity  $\epsilon_0$ , taking into account a typical effective polarizability of the remaining valence electrons that lowers the double ionization threshold.<sup>25</sup> Thus, considering typical  $\sim 10$  eV ionization potential and  $R$  on the order of 1 Å, EUV photon energies as low as 35 eV can be used to induce CE and serve as a general probe of molecular structure. Free electron laser (FEL) facilities

<sup>a</sup> Institute of Chemistry, The Hebrew University of Jerusalem, Jerusalem, 91904, Israel. E-mail: strasser@huji.ac.il

<sup>b</sup> Fritz Haber Center for Molecular Dynamics, Institute of Chemistry, The Hebrew University of Jerusalem, Jerusalem, 91904, Israel

presently provide tunable wavelength and sub picoseconds timing of EUV and soft X-ray pulses. Furthermore, tabletop high order harmonic generation (HHG) setups allow producing coherent broad bandwidth EUV bursts, regularly implemented in fs pump-probe experiments,<sup>28–35</sup> and supporting attosecond pulse trains.<sup>28</sup> These emerging ultrafast EUV and soft X-ray sources make it appealing to attempt visualizing time resolved structural dynamics by single-photon CE. Interestingly, while the broad bandwidth of attosecond EUV bursts limits the resolution of methods such as photoelectron spectroscopy,<sup>29</sup> the KER of the ionic products can be expected to be less sensitive to the excess energy of the ionizing photon which is carried away by the emitted photoelectrons.

Intense EUV pulses available at leading FEL facilities enable non-linear processes at EUV photon energies, such as sequential multiple ionization.<sup>36–38</sup> Recently utilized in time resolved CE probing of dynamics on a sub picoseconds time scale.<sup>38,39</sup> Probing dynamics of cations by time delayed photoionization and CE was also demonstrated in FEL EUV pump-EUV probe studies,<sup>36,37,40</sup> as well as cutting edge HHG pump-intense field probe studies.<sup>33–35,41</sup> However, to the best of our knowledge there are no previous attempts to take advantage of the rare single-photon CE events to probe neutral molecules using the low flux table top HHG sources, which produce broad bandwidth attosecond pulse trains. Implementing a single-photon CE probe using HHG attosecond pulse source presents significant experimental and conceptual challenges: the experimental challenge is due to the rare occurrence of single-photon CE compared to dissociative ionization. The conceptual challenges are due the possibility of a step-wise double ionization involving dynamics on autoionizing cation intermediates, as well as due to the sheer broad bandwidth of the attosecond pulse train.

In this manuscript we present 3D coincidence imaging measurements of the single-photon CE of CH<sub>3</sub>OH methanol molecules, initiated with a broad bandwidth HHG attosecond pulse train of EUV bursts. The different CE channels are identified and successfully disentangled from the predominant dissociative ionization background processes. KER and angular distributions are presented and directly compared to previous CE measurements of methanol using either intense field or using narrow bandwidth continuous sources.<sup>18,26</sup> Furthermore, *ab initio* calculations of the dication system are presented to explain the measured KER.

## Experimental scheme

Fig. 1 shows a schematic representation of the experimental scheme. Ultrafast EUV pulses are generated at 1 kHz repetition rate by focusing sub 35 fs, 800 nm laser<sup>42</sup> pulses in a semi-infinite HHG cell filled with few torr Neon.<sup>43</sup> About 50% of the amplified laser pulse energy (total 3.2 mJ) is used to achieve  $\sim 2 \times 10^{15}$  W cm<sup>-2</sup> in the HHG cell, while the remaining 50% of the pulse energy are split and redirected to be used as pump in pump-probe studies. HHG was optimized on single photon double ionization of Neon confirming efficient production of EUV above the 63 eV double ionization threshold energy

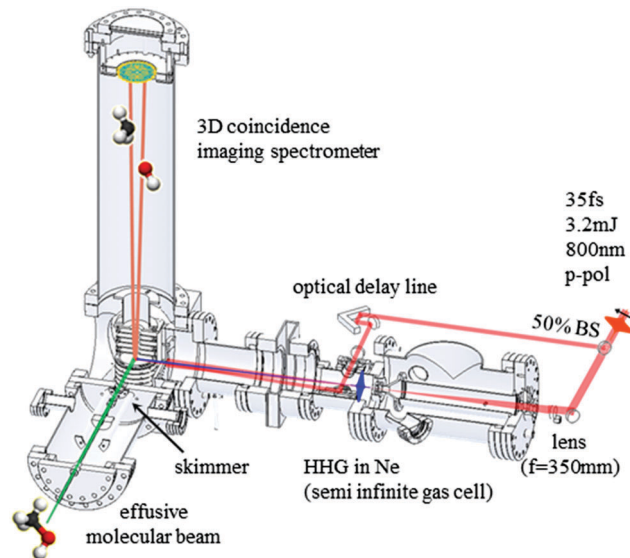


Fig. 1 Schematic representation of the single-photon CE setup.

of Neon.<sup>44</sup> Thus adequate for double ionization of all simple molecules of interest.<sup>25</sup> A dedicated 3D coincidence fragment imaging spectrometer is positioned  $\sim 700$  mm after the HHG region, such that the near-IR pulse is defocused and spatially filtered from lower divergence HHG.<sup>45</sup> Thus the entire HHG spectrum supporting attosecond pulse trains is utilized for single-photon CE. At the center of the spectrometer, the HHG pulse crosses a skimmed effusive beam of methanol vapor. Spectrometer potentials are optimized for velocity map imaging conditions,<sup>46</sup> accelerating cation products towards a time and position sensitive MCP detector, equipped with a P46 phosphor anode. For each HHG shot, the 2D hit positions are read out using CCD cameras, while the timing signal is digitized by a fast scope. More detailed description of our data acquisition scheme was previously described by Kandhasamy *et al.*<sup>47</sup> 3D velocities of the detected fragments are calculated based on high resolution SIMION trajectory simulations. The total momentum conservation is restricted using center of mass cut. This restriction allows suppressing the random coincidence background from dissociative ionization events by more than a factor of 30, depending on the specific CE channel. Most of the remaining background is concentrated around zero KER, clearly separated from the high KER CE events of interest. For the  $\sim 3$  counts per 100 shots rate used in this study, the random coincidence background contribution near zero KER amounts to only few percent of CE yield and is subtracted from the presented KER. It is therefore possible to increase the count rate and significantly reduce the 7 day integration time, while still allowing analysis of minority CE channels such as proton migration to form H<sub>2</sub>O<sup>+</sup>.

## Results and discussion

The broad bandwidth of a HHG attosecond pulse train produces a variety of dissociative ionization channels that dominate the cationic fragment spectrum of a methanol molecule.<sup>22</sup> The full

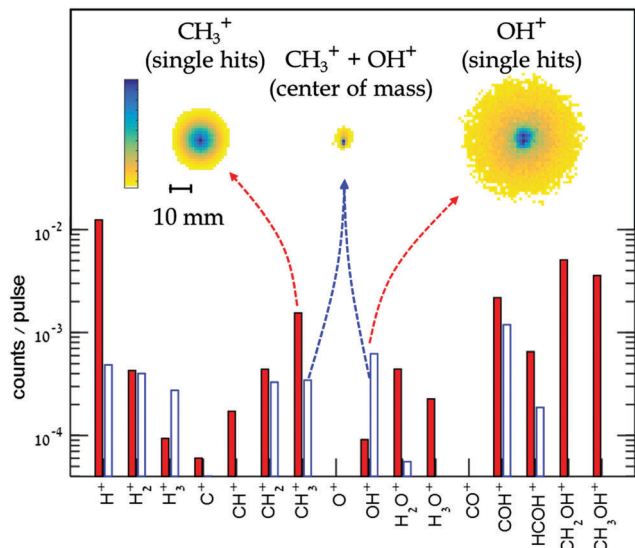


Fig. 2 Full bars indicate cation count rates evaluated from single cation hits of the relevant dissociative ionization product. Empty bars indicate the coincidence count rates from single-photon CE events (scaled by  $\times 100$ ). Left and right insets show distributions of  $\text{CH}_3^+$  and  $\text{OH}^+$  fragments (respectively) on the 2D detector plane, while center inset shows the distribution of center of mass positions on the detector plane for  $\text{CH}_3^+$  and  $\text{OH}^+$  detected in coincidence.

bars in Fig. 2 show the measured cation yields, dominated by  $\text{CH}_2\text{OH}^+$ ,  $\text{HCOH}^+$ ,  $\text{COH}^+$ ,  $\text{CH}_3^+$  and  $\text{H}^+$ . Fig. 2 insets show typical hit distributions on the 2D detector plane for single hits of  $\text{CH}_3^+$  or  $\text{OH}^+$  cations. Taking advantage of the relatively low flux of the HHG light source, the total ionization probabilities are kept below 3%, minimizing random coincidence of cations from separate molecules. True single-photon CE events (presented by the empty bars in Fig. 2) are disentangled from the dissociative ionization background by 3D coincidence detection of all the cationic products and requiring strict total momentum conservation. Fig. 2 inset show a typical center of mass hit position distribution on the 2D detector plane, calculated for  $\text{CH}_3^+$  and  $\text{OH}^+$  cations detected in coincidence. The narrow center of mass distribution limited mainly by the velocity spread in the methanol sample allow rejection of random coincidence events or events arriving from impurities such as methanol clusters. On average, CE is found only in less than 0.1% of the total photoionization events, suggesting an overwhelming signal to background ratio. Nevertheless, while ion species such as  $\text{H}^+$ ,  $\text{CH}^+$  and  $\text{H}_3\text{O}^+$  are produced mostly in dissociative ionization events, the relative CE fraction is significantly enhanced up to  $\sim 2.5\%$  for  $\text{H}_3^+$  and  $\sim 7\%$  for the  $\text{OH}^+$  products. Thus, mass resolved coincidence detection allows characterization of specific single-photon CE channels, disentangled from dissociative ionization. Fully detected CE channels of  $\text{CH}_3^+ + \text{OH}^+$ ,  $\text{H}_3^+ + \text{COH}^+$ ,  $\text{H}_2^+ + \text{HCOH}^+$  and  $\text{CH}_2^+ + \text{H}_2\text{O}^+$  are detected at respective rates of 3.8, 2.7, 1.1 and 0.6 events per  $10^6$  HHG shots ( $\sim 16$  min integration time at a 1 kHz repetition rate), allowing feasible measurement times. Partially detected CE events involving two detected cations and an undetectable neutral product, such as  $\text{CH}_2^+ + \text{OH}^+ + \text{H}$  and  $\text{H}_2^+ + \text{COH}^+ + \text{H}$

are also observed. However, 3-body analysis, considering the missing momentum due to the undetected neutral product recoil is beyond the scope of this work concentrating only on fully detected two-body CE.

Fig. 3a shows the KER distribution measured for the predominant  $\text{CH}_3\text{OH}^{2+} \rightarrow \text{CH}_3^+ + \text{OH}^+$  single-photon CE channel, breaking the C–O bond. The KER distribution peaks at about  $\sim 6.4$  eV and extends from 4 eV until  $\sim 11$  eV. The KER is

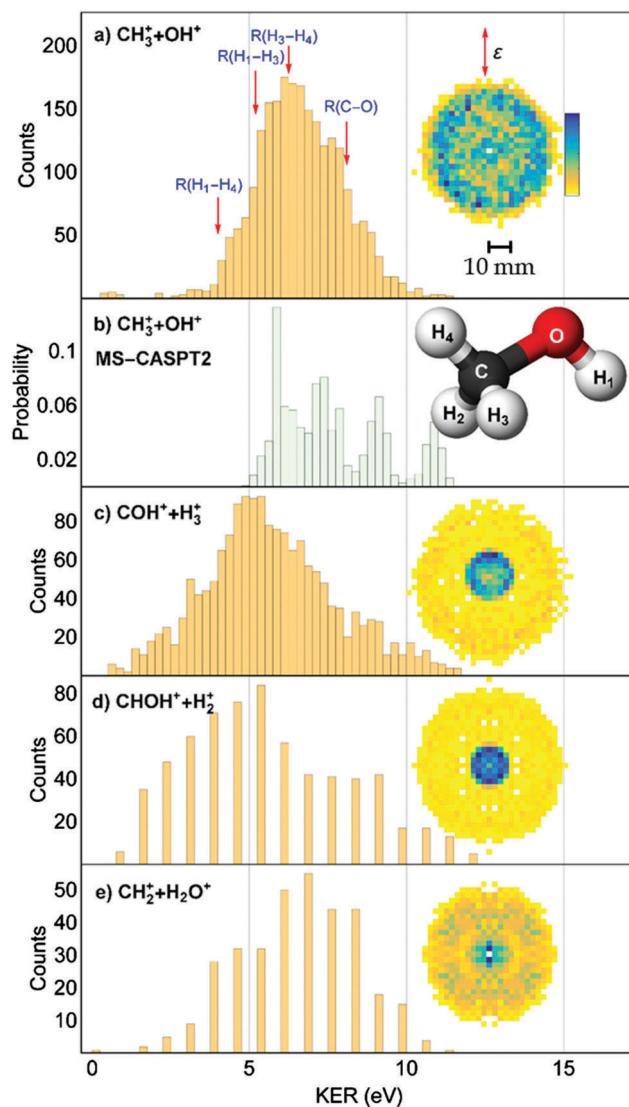


Fig. 3 KER distributions for the 2-body single-photon CE of methanol for the following channels: panels (a) and (c–e) show experimental results for the  $\text{CH}_3^+ + \text{OH}^+$ ,  $\text{COH}^+ + \text{H}_3^+$ ,  $\text{CHOH}^+ + \text{H}_2^+$  and  $\text{CH}_2^+ + \text{H}_2\text{O}^+$  respectively. In each panel an inset shows the measured KER distribution and angular resolved fragment hit distributions on the 2D detector plane, when for the less abundant  $\text{CHOH}^+ + \text{H}_2^+$  and  $\text{CH}_2^+ + \text{H}_2\text{O}^+$  channels the angular distribution is symmetrized relative to a vertical laser polarization. In the position distributions of channels  $\text{COH}^+ + \text{H}_3^+$  and  $\text{CHOH}^+ + \text{H}_2^+$  the high recoil for the low mass and low recoil of the high mass are clearly resolved. Panel (b) shows the KER distribution estimated for the  $\text{CH}_3^+ + \text{OH}^+$  channel by the theoretical model. KER values, indicated by arrows in panel (a) are estimated using a simple model based on possible inter-charge distances within the neutral methanol geometry.

therefore in rough agreement with the 5.9 eV KER estimate based on coincidence time of flight measurements performed with a 30.4 nm narrow bandwidth source.<sup>48</sup>

The most probable KER observed with intense field CE in the  $\text{CH}_3^+ - \text{OH}^+$  channel was reported to depend on the specific peak intensity and time duration of the intense pulse.<sup>18,19</sup> For example lower KER of  $\sim 5$  eV was reported with 60 fs pulses, increasing to  $\sim 6$  eV for 7 fs pulse duration.<sup>18</sup> The KER peak energy reported for intense field CE using shorter laser pulses is closer to the single-photon CE peak presented here, supporting the intuitive notion that shorter intense field pulses approach asymptotically to an instantaneous double ionization. However, the intense field CE KER peak was also demonstrated to shift towards higher energies with increasing peak intensity at a fixed pulse duration.<sup>19</sup>

Fig. 3a inset shows the angular resolved fragment hit distribution on the 2D detector plane, showing nearly isotropic angular distribution with respect to the indicated laser polarization angle. In contrast, strong sensitivity to molecular alignment was reported for intense field CE of methanol, with special preference to an average  $39^\circ$  or  $0^\circ$  angle of the broken C–O bond with respect to the laser polarization, depending on the respective 7 or 21 fs laser pulse duration.<sup>18</sup> One could expect the single-photon CE cross-section to exhibit a non-trivial dependence on the molecular alignment with respect to the laser polarization, with a different angular dependence for different photon energies.<sup>49,50</sup> Thus, the broad bandwidth HHG pulse can contribute to the observed nearly isotropic single-photon CE probability, independent of molecular alignment.

In contrast to other methods, such as photoelectron spectroscopy, the width of the measured KER peak does not reflect the light source bandwidth. Thus, the FWHM of the measured peak is only  $\sim 3$  eV while the HHG attosecond pulse train producing double ionization spans a bandwidth exceeding 30 eV. The excess energy of the pulse train is taken by the electrons released into the continuum. As single-photon CE occurs under low field conditions it is valuable to perform *ab initio* calculations of the  $\text{CH}_3\text{OH}^{2+}$  dynamics, under the assumption of instantaneous double ionization, in order to explain the observed KER in the predominant C–O bond breaking single-photon CE channel. Our first attempt at understanding the CE dynamics involved performing *ab initio* molecular dynamics (AIMD) trajectories on the singlet and triplet dication ground states at the restricted active space multiconfigurational self-consistent-field (RASSCF) level. The calculations employed the MOLCAS program including an active space containing 12 electrons in 10 orbitals.<sup>51</sup> These trajectories are initiated from phase space configurations sampled from the neutral ground state AIMD trajectories at 300 K, assuming instantaneous double ionization. On the singlet potential,  $\text{H}^+$  and  $\text{H}_3^+$  products are observed following fragmentation of the methyl group. Contrarily, the dynamics on the triplet potential, while involving energy dissipation into proton motion, did not exhibit fragmentation within the 200 fs timescale of the calculated trajectories.

In order to understand the lack of CO bond breaking in the molecular dynamics on the dication potential energy surfaces

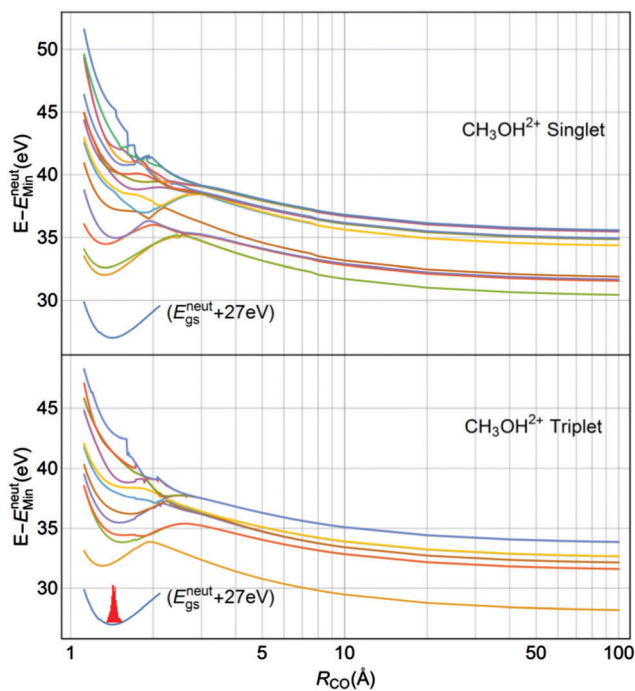


Fig. 4 The potential energy curves of methanol dication calculated using MS-CASPT2. The calculations were performed using MOLCAS and the active space included 12 electrons on 10 orbitals.<sup>51</sup> Also shown, the neutral ground state curve and a histogram of the CO bond length distribution, determined by an AIMD trajectory at 300 K.

(PESs), we calculated the potential energy curves of the ground and excited singlet and triplet states as a function of the C–O distance  $R_{\text{CO}}$  (freezing all internal degrees of freedom within the  $\text{CH}_3^+$  and  $\text{OH}^+$  fragments) shown in Fig. 4. The calculated dication potentials converge at large  $R_{\text{CO}}$  distances to Coulombic repulsion curves, leading asymptotically to different electronic states of the  $\text{CH}_3^+$  and  $\text{OH}^+$  dissociation products.

One notable feature in Fig. 4 is that both the singlet and triplet ground and low-lying excited states exhibit a  $>2$  eV barrier for dissociation at  $R_{\text{CO}} \approx 2\text{--}3$  Å. The existence of the barrier can be understood using Mulliken population analysis, finding that in the Franck–Condon region the  $\text{CH}_3$  fragment carries most of the dication positive charge. Obviously, CE will occur only if the positive charge is shared equally by the  $\text{CH}_2$  and  $\text{OH}$  fragments. Hence the route to CE involves a hole transfer from  $\text{CH}_3$  to  $\text{OH}$  as the two fragments dissociate, a feat requiring an activation energy, resulting in the formation of the potential barrier. For higher excited states the potential energy at the FC region is sufficient for prompt dissociation, through a series of non-adiabatic crossings to lower adiabatic states. Obviously, a correct account of the CE dynamics requires a multidimensional quantum mechanical non-adiabatic treatment and is beyond the scope of this work. Nevertheless, it is possible to estimate KER distributions by assuming instantaneous projection from neutral ground state (GS) geometries onto the excited dication potentials, followed by prompt above the barrier breaking of the C–O bond while neglecting energy dissipation into the other ro-vibrational degrees of freedom.

We assumed a probability of unity for all non-adiabatic transitions (consistent with the calculated Landau-Zener transition probabilities), taking advantage of the fact that all adiabatic energy differences in the avoided crossing regions are small. The resulting KER distribution is shown in Fig. 3b and can be directly compared to the experimental measurement shown in Fig. 3a. The four peaks correspond to different excited state potentials correlating to distinct electronically excited dissociation products. The peaks are further broadened due to the steep gradient of the excited states, coupled with the distribution of initial geometries sampled from the AIMD trajectory on the neutral ground state at 300 K.

The measured KER range is successfully reproduced by the calculated KER distribution described above, supporting the assumption of an instantaneous double ionization that is followed by prompt dissociation. The KER distribution exhibits higher probability around the peak of the experimental spectrum although the calculation considers equal contributions from the possible dication states. The relative populations of different excited states depend on the electron-electron correlation that facilitates double ionization with a single EUV photon.<sup>27,41,50</sup> The relatively lower probability of events with KER above 10 eV could in fact reflect a lower contribution from the high lying states associated with correspondingly high KER. The theoretical results neglect dissipation of energy into vibrational and rotational degrees of freedom and this is likely the reason for the measured KER events below 5 eV that do not appear in the calculated spectrum.

Fig. 3c shows the KER distribution of the second most intense single-photon CE channel that breaks all three C-H bonds on the methyl group to form a  $\text{H}_3^+$  cation. The KER distribution for the  $\text{H}_3^+ - \text{COH}^+$  channel is shifted towards lower KER compared with the C-O bond breaking channel. The broad KER peak centered at about 5 eV is significantly higher than the KER reported for a similar final channel, producing  $\text{H}_3^+$  by highly charged ion collision with methanol.<sup>52</sup> Similarly to the  $\text{CH}_3^+ + \text{OH}^+$  channel, the angular resolved fragment hit distribution on the 2D detector plane shown in Fig. 3c inset is rather isotropic. The heavier  $\text{COH}^+$  fragments are concentrated in the center of the detector, while the lighter  $\text{H}_3^+$  recoil away, carrying most of the KER.

$\text{H}_3^+$  emission from intense field CE was also reported to exhibit a broad KER distribution around 4.5 eV with an isotropic distribution with respect to the laser polarization.<sup>53</sup> The isotropic angular distribution was initially interpreted as indication for a long lived ( $> 1.4$  ps) transient dication.<sup>53</sup> However, theoretical calculations support a rapid two step mechanism for  $\text{H}_3^+$  formation: first separation of a neutral  $\text{H}_2$  system from the dication, followed by proton transfer within less than 300 fs even in deuterated methanol.<sup>54</sup> This  $\text{H}_3^+$  formation mechanism is also observed in our AIMD trajectories calculated on the singlet dication GS.

Fig. 3d shows a smaller single-photon CE channel, in which  $\text{H}_3^+$  is not formed and a  $\text{H}_2^+$  cation breaks away from the methanol system. Significant yield is also observed for partially detected  $\text{H} + \text{H}_2^+ + \text{COH}^+$  channel, in which although all three

C-H bonds break the stable  $\text{H}_3^+$  formation is not successful. In our trajectory calculations,  $\text{H}_2^+$  formation was not observed on the singlet GS. It is therefore possible that  $\text{H}_2^+$  formation in 2 or 3 body fragmentation processes occurs on the GS at longer time scales or due to complex dynamics on higher excited states.

A particularly interesting single-photon CE channel involves proton migration from the methyl to form a water cation and a  $\text{CH}_2^+$  fragment. Fig. 3e shows the KER distribution for these rare events, which in our measurements are observed for only  $\sim 4\%$  of all CE. Interestingly, the KER peak for these proton migration events is shifted towards higher KER compared to the C-O bond breaking channel. The higher KER tentatively corresponds to dissociation on highly excited dication states, in accord with no proton migration trajectories on the dication GSs. In contrast, calculations on singly ionized methanol GS were reported to exhibit efficient proton migration.<sup>54</sup> In fact, intense field CE was reported to exhibit higher branching ratios of proton migration *versus* C-O bond breaking channel, ranging from 0.5 to 0.13 depending on the intense pulse parameters.<sup>18,19</sup> For the relatively long 60 fs and 40 fs pulses, it is reasonable that the higher proton migration branching ratio in intense field CE stems from the time spent on the singly ionized potential, which is assumed not to be populated during single-photon CE. Nevertheless, it is valuable to note that intense field CE with the 7 fs pulses was reported to show 0.17 branching ratio of proton migration *versus* C-O bond breaking, while intense field CE with longer 21 fs pulses were reported to exhibit 0.13 branching ratio,<sup>18</sup> same as proton migration following single photon CE. Thus minimization of sequential ionization effects by considering the asymptotic intense field CE behavior at short pulse durations does not necessarily converge to an instantaneous low field multiple ionization achieved by single-photon CE.

One must keep in mind that as opposed to foil CEI experiments, not all valence electrons are removed by a single EUV photon and that the detected products are molecular cations. It is therefore naive to directly assign an internuclear  $R(\text{C-O})$  distance according to a purely Coulombic repulsive potential between two point charges, as evident from the calculated potentials shown in Fig. 4. Intuitively, the excess positive charge of the methanol dication is more likely to be concentrated near the protons. Furthermore, in the early stages of dissociation the remaining valence electrons act to screen the excess positive charge, reducing the potential energy of the doubly ionized system. In the following we offer an alternative approach that can be used in the absence of calculated potentials to provide an estimate for CE KER based on a simple tentative rule of thumb. We propose to extend the empiric threshold law of Eland *et al.*<sup>25</sup> that successfully describes the threshold energy for single photon double ionization of many simple molecules using an effective permittivity  $\epsilon = 1.25\epsilon_0$ .<sup>25</sup> The potential energy that can be released as KER can therefore be estimated by  $1/(4\pi\epsilon R)$ , where  $R$  is an effective inter-charge distance. The arrows in Fig. 3a indicate the thus estimated KER, taking into account the different possible proton-proton distances in the neutral methanol GS geometry shown in Fig. 3b.

An additional arrow indicates a limit assuming an inter-charge distance corresponding to the C–O bond length. Thus, both width and position of the measured KER peak, corresponding to prompt cleavage of the C–O bond, are in agreement also with a simple tentative guess for the possible inter-charge distances.

## Conclusions

Single-photon CE of methanol molecules is performed with the full broad bandwidth of a HHG attosecond pulse train, paving the way for time resolved imaging of ultrafast changes in the molecular structure. In contrast to narrow bandwidth continuous light sources that were previously used for single photon double ionization, the presented work takes advantage of the full bandwidth produced by HHG. Nevertheless, the observed KER spread of specific single-photon CE channels is by no means limited by the high bandwidth supporting attosecond pulses, as the excess energy is carried away by the ejected electrons. Four dominant two-body single-photon CE channels are clearly observed and disentangled from the dissociative ionization background by 3D coincidence imaging of one methanol molecule at a time. AIMD calculations indicate that the predominant C–O bond breaking single-photon CE channel does not occur on the dication GS due a potential barrier. Nevertheless, excited state potentials allow accounting for the measured KER spectrum, peaking at  $\sim 6.4$  eV and extending from 4 eV to  $\sim 11$  eV, by assuming instantaneous double ionization followed by prompt dissociation above the barrier. Furthermore, a simple model is proposed for estimating the KER based on tentative inter-charge distances within the neutral molecule geometry. More theoretical and experimental work is necessary to test the validity of the simple assumptions that are successful in describing the measured KER in the C–O bond breaking single-photon CE of methanol.

CE channels that involve breaking 2 or 3 of the C–H bonds are observed to exhibit lower KER, in agreement with an intricate hydrogen motion leading to  $\text{H}_3^+$  or  $\text{H}_2^+$  formation. In contrast, higher KER is observed for C–O bond breaking that is accompanied with proton migration, indicating the role of highly excited dication states.

The agreement of the calculated KER distribution for the C–O breaking single-photon CE channel with the experimental measurement supports an instantaneous double ionization of the molecule, followed by prompt dissociation. Furthermore, the nearly isotropic response of the broad bandwidth single-photon CE makes it ideally suitable as a time resolved probe that does not suffer from geometric alignment<sup>55,56</sup> or requires special preparation of the evolving molecular system in an aligned state.<sup>57</sup> Although description of the single photon double ionization mechanism for producing excited dication states is beyond the scope of this work, its strong dependence on electron correlation can be potentially used to reflect attosecond electron wavepacket dynamics in time resolved single-photon CE measurements using broad bandwidth HHG pulses.

## Acknowledgements

DS gratefully acknowledge financial assistance from the European Research Council through grant number 306783. RB gratefully acknowledges support from the Israel Science Foundation grant no. 189/14.

## Notes and references

- 1 A. H. Zewail, *J. Phys. Chem. A*, 2000, **104**, 5660–5694.
- 2 K. Yamanouchi, *Science*, 2002, **295**, 1659–1660.
- 3 O. Gessner, *Science*, 2006, **311**, 219–222.
- 4 P. Herwig, K. Zawatzky, M. Grieser, O. Heber, B. Jordon-Thaden, C. Krantz, O. Novotny, R. Repnow, V. Schurig, D. Schwalm, Z. Vager, A. Wolf, O. Trapp and H. Kreckel, *Science*, 2013, **342**, 1084–1086.
- 5 D. Strasser, L. Lammich, S. Krohn, M. Lange, H. Kreckel, J. Levin, D. Schwalm, Z. Vager, R. Wester, a. Wolf and D. Zajfman, *Phys. Rev. Lett.*, 2001, **86**, 779–782.
- 6 Z. Vager, R. Naaman and E. P. Kanter, *Science*, 1989, **244**, 426–431.
- 7 H. Stapelfeldt, E. Constant and P. B. Corkum, *Phys. Rev. Lett.*, 1995, **74**, 3780–3783.
- 8 S. Chelkowski, P. B. Corkum and A. D. Bandrauk, *Phys. Rev. Lett.*, 1999, **82**, 3416–3419.
- 9 S. Kim, E. Brostromer, D. Xing, J. Jin, S. Chong, H. Ge, S. Wang, C. Gu, L. Yang, Y. Q. Gao, X.-d. Su, Y. Sun and X. S. Xie, *Science*, 2013, **339**, 816–819.
- 10 D. E. Folmer, E. S. Wisniewski, S. M. Hurley and A. W. Castleman, *Proc. Natl. Acad. Sci. U. S. A.*, 1999, **96**, 12980–12986.
- 11 D. E. Folmer, E. S. Wisniewski and A. W. Castleman, *Chem. Phys. Lett.*, 2000, **318**, 637–643.
- 12 D. E. Folmer, L. Poth, E. S. Wisniewski and A. W. Castleman, *Chem. Phys. Lett.*, 1998, **287**, 1–7.
- 13 J. Catalán, J. C. del Valle and M. Kasha, *Chem. Phys. Lett.*, 2000, **318**, 629–636.
- 14 J. Catalán, J. C. del Valle and M. Kasha, *Proc. Natl. Acad. Sci. U. S. A.*, 1999, **96**, 8338–8343.
- 15 L. J. Frasinski, J. Plumridge, J. H. Posthumus, K. Codling, P. F. Taday, E. J. Divall and a. J. Langley, *Phys. Rev. Lett.*, 2001, **86**, 2541–2544.
- 16 A. S. Alnaser, X. M. Tong, T. Osipov, S. Voss, C. M. Maharjan, P. Ranitovic, B. Ulrich, B. Shan, Z. Chang, C. D. Lin and C. L. Cocke, *Phys. Rev. Lett.*, 2004, **93**, 183202.
- 17 T. Ergler, A. Rudenko, B. Feuerstein, K. Zrost, C. D. Schröter, R. Moshhammer and J. Ullrich, *Phys. Rev. Lett.*, 2005, **95**, 93001.
- 18 R. Itakura, P. Liu, Y. Furukawa, T. Okino, K. Yamanouchi and H. Nakano, *J. Chem. Phys.*, 2007, **127**, 104306.
- 19 H. Xu, T. Okino, T. Kudou, K. Yamanouchi, S. Roither, M. Kitzler, A. Baltuska and S. L. Chin, *J. Phys. Chem. A*, 2012, **116**, 2686–2690.
- 20 B. Yang, L. Zhang, H. Xu, R. Li and K. Yamanouchi, *Chin. J. Physiol.*, 2014, **52**, 652–674.
- 21 T. Weber, A. O. Czasch, O. Jagutzki, A. K. Müller, V. Mergel, A. Kheifets, E. Rotenberg, G. Meigs, M. H. Prior, S. Daveau,

- A. Landers, C. L. Cocke, T. Osipov, R. Díez Muiño, H. Schmidt-Böcking and R. Dörner, *Nature*, 2006, **443**, 1014.
- 22 K. Ueda and J. H. Eland, *J. Phys. B: At., Mol. Opt. Phys.*, 2005, **38**, S839–S859.
- 23 T. Weber, a. O. Czasch, O. Jagutzki, a. K. Müller, V. Mergel, A. Kheifets, E. Rotenberg, G. Meigs, M. H. Prior, S. Daveau, A. Landers, C. L. Cocke, T. Osipov, R. Díez Muiño, H. Schmidt-Böcking and R. Dörner, *Nature*, 2006, **443**, 1014.
- 24 J. H. D. Eland, *Chem. Phys.*, 2003, **294**, 171–186.
- 25 R. D. Molloy, A. Danielsson, L. Karlsson and J. H. D. Eland, *Chem. Phys.*, 2007, **335**, 49–54.
- 26 P. Linusson, M. Stenrup, Å. Larson, E. Andersson, F. Heijkenskjöld, P. Andersson, J. H. Eland, L. Karlsson, J.-E. Rubensson and R. Feifel, *Phys. Rev. A: At., Mol., Opt. Phys.*, 2009, **80**, 1–6.
- 27 B. Gaire, S. Y. Lee, D. J. Haxton, P. M. Pelz, I. Bocharova, F. P. Sturm, N. Gehrken, M. Honig, M. Pitzer, D. Metz, H. K. Kim, M. Schoffler, R. Dörner, H. Gassert, S. Zeller, J. Voigtsberger, W. Cao, M. Zohrabi, J. Williams, A. Gatton, D. Reedy, C. Nook, T. Moller, A. L. Landers, C. L. Cocke, I. Ben-Itzhak, T. Jahnke, A. Belkacem and T. Weber, *Phys. Rev. A: At., Mol., Opt. Phys.*, 2014, **89**, 1–16.
- 28 P. Antoine, A. L'Huillier and M. Lewenstein, *Phys. Rev. Lett.*, 1996, **77**, 1234–1237.
- 29 D. Strasser, F. Goulay and S. R. Leone, *J. Chem. Phys.*, 2007, **127**, 184305.
- 30 D. Strasser, L. H. Haber, B. Doughty and S. R. Leone, *Mol. Phys.*, 2008, **106**, 275–280.
- 31 T. Pfeifer, C. Spielmann and G. Gerber, *Rep. Prog. Phys.*, 2006, **69**, 443–505.
- 32 X. Zhou, P. Ranitovic, C. W. Hogle, J. H. Eland, H. C. Kapteyn and M. M. Murnane, *Nat. Phys.*, 2012, **8**, 232–237.
- 33 E. Gagnon, P. Ranitovic, X.-M. M. Tong, C. L. Cocke, M. M. Murnane, H. C. Kapteyn and A. S. Sandhu, *Science*, 2007, **317**, 1374–1378.
- 34 W. Cao, S. De, K. P. Singh, S. Chen, M. S. Schöffler, A. S. Alnaser, I. A. Bocharova, G. Laurent, D. Ray, S. Zherebtsov, M. F. Kling, I. Ben-Itzhak, I. V. Litvinyuk, A. Belkacem, T. Osipov, T. Rescigno and C. L. Cocke, *Phys. Rev. A: At., Mol., Opt. Phys.*, 2010, **82**, 3–7.
- 35 J. Rothhardt, S. Hädrich, Y. Shamir, M. Tschernajew, R. Klas, A. Hoffmann, G. K. Tadesse, A. Klenke, T. Gottschall, T. Eidam, J. Limpert, A. Tünnermann, R. Boll, C. Bomme, H. Dachraoui, B. Erk, M. Di Fraia, D. A. Horke, T. Kierspel, T. Mullins, A. Przystawik, E. Savel'yev, J. Wiese, T. Laarmann, J. Küpper and D. Rolles, *Opt. Express*, 2016, **24**, 18133.
- 36 O. Kornilov, M. Eckstein, M. Rosenblatt, C. P. Schulz, K. Motomura, A. Rouzée, J. Klei, L. Foucar, M. Siano, A. Lübcke, F. Schapper, P. Johnsson, D. M. P. Holland, T. Schlathölter, T. Marchenko, S. Düsterer, K. Ueda, M. J. J. Vrakking and L. J. Frasinski, *J. Phys. B: At., Mol. Opt. Phys.*, 2013, **46**, 164028.
- 37 Y. H. Jiang, A. Rudenko, M. Kurka, K. U. Kühnel, T. Ergler, L. Foucar, M. Schöffler, S. Schössler, T. Havermeier, M. Smolarski, K. Cole, R. Dörner, S. Düsterer, R. Treusch, M. Gensch, C. D. Schröter, R. Moshhammer and J. Ullrich, *Phys. Rev. Lett.*, 2009, **102**, 123002.
- 38 A. Rouzée, P. Johnsson, L. Rading, A. Hundertmark, W. Siu, Y. Huismans, S. Düsterer, H. Redlin, F. Tavella, N. Stojanovic, A. Al-Shemmary, F. Lépine, D. M. P. Holland, T. Schlathölter, R. Hoekstra, H. Fukuzawa, K. Ueda and M. J. J. Vrakking, *J. Phys. B: At., Mol. Opt. Phys.*, 2013, **46**, 164029.
- 39 V. S. Petrović, M. Siano, J. L. White, N. Berrah, C. Bostedt, J. D. Bozek, D. Broege, M. Chalfin, R. N. Coffee, J. Cryan, L. Fang, J. P. Farrell, L. J. Frasinski, J. M. Glowia, M. Gühr, M. Hoener, D. M. P. Holland, J. Kim, J. P. Marangos, T. Martinez, B. K. McFarland, R. S. Minns, S. Miyabe, S. Schorb, R. J. Sension, L. S. Spector, R. Squibb, H. Tao, J. G. Underwood and P. H. Bucksbaum, *Phys. Rev. Lett.*, 2012, **108**, 253006.
- 40 N. Berrah, J. Bozek, J. T. Costello, S. Düsterer, L. Fang, J. Feldhaus, H. Fukuzawa, M. Hoener, Y. H. Jiang, P. Johnsson, E. T. Kennedy, M. Meyer, R. Moshhammer, P. Radcliffe, M. Richter, A. Rouzée, A. Rudenko, A. a. Sorokin, K. Tiedtke, K. Ueda, J. Ullrich and M. J. J. Vrakking, *J. Mod. Opt.*, 2010, **57**, 1015–1040.
- 41 E. P. Månsson, D. Guénot, C. L. Arnold, D. Kroon, S. Kasper, J. M. Dahlström, E. Lindroth, A. S. Kheifets, A. L. Huillier, S. L. Sorensen and M. Gisselbrecht, *Nat. Phys.*, 2014, **10**, 207–211.
- 42 Spitfire pro XP; Spectra-Physics; Newport Co.
- 43 J. Sutherland, E. Christensen, N. Powers, S. Rhynard, J. Painter and J. Peatross, *Opt. Express*, 2004, **12**, 4430–4436.
- 44 R. I. Hall, A. McConkey, K. Ellis, G. Dawber, M. a. MacDonald and G. C. King, *J. Phys. B: At., Mol. Opt. Phys.*, 1999, **25**, 799–810.
- 45 J. P. Brichta, M. C. H. Wong, J. B. Bertrand, H. C. Bandulet, D. M. Rayner and V. R. Bhardwaj, *Phys. Rev. A: At., Mol., Opt. Phys.*, 2009, **79**, 33404.
- 46 A. T. J. B. Eppink and D. H. Parker, *Rev. Sci. Instrum.*, 1997, **68**, 3477.
- 47 D. M. Kandhasamy, Y. Albeck, K. Jagtap and D. Strasser, *J. Phys. Chem. A*, 2015, **119**, 8076–8082.
- 48 J. H. Eland and B. J. Treves-Brown, *Int. J. Mass Spectrom. Ion Processes*, 1992, **113**, 167–176.
- 49 M. Alagia, P. Candori, S. Falcinelli, M. Lavollée, F. Pirani, R. Richter, S. Stranges and F. Vecchiocattivi, *Phys. Chem. Chem. Phys.*, 2010, **12**, 5389.
- 50 B. Gaire, A. Gatton, F. Wiegandt, J. Neff, C. Janke, S. Zeller, D. Reedy, J. Rajput, I. Ben-Itzhak, A. L. Landers, A. Belkacem and T. Weber, *Phys. Rev. A: At., Mol., Opt. Phys.*, 2016, **94**, 33412.
- 51 F. Aquilante, J. Autschbach, R. K. Carlson, L. F. Chibotaru, M. G. Delcey, L. De Vico, I. Fdez. Galvan, N. Ferre, L. M. Frutos, L. Gagliardi, M. Garavelli, A. Giussani, C. E. Hoyer, G. Li Manni, H. Lischka, D. Ma, P. A. Malmqvist, T. Muller, A. Nenov, M. Olivucci, T. B. Pedersen, D. Peng, F. Plasser, B. Pritchard, M. Reiher, I. Rivalta, I. Schapiro, J. Segarra-Martí, M. Stenrup, D. G. Truhlar, L. Ungur, A. Valentini, S. Vancollie, V. Veryazov, V. P. Vysotskiy, O. Weingart, F. Zapata and R. Lindh, *J. Comput. Chem.*, 2016, **37**, 506–541.

- 52 S. De, J. Rajput, A. Roy, P. N. Ghosh and C. P. Safvan, *Phys. Rev. Lett.*, 2006, **97**, 1–4.
- 53 T. Okino, Y. Furukawa, P. Liu, T. Ichikawa, R. Itakura, K. Hoshina, K. Yamanouchi and H. Nakano, *Chem. Phys. Lett.*, 2006, **419**, 223–227.
- 54 K. Nakai, T. Kato, H. Kono and K. Yamanouchi, *J. Chem. Phys.*, 2013, **139**, 3–7.
- 55 J. H. Posthumus, J. Plumridge, M. K. Thomas, K. Codling, L. J. Frasinski, a. J. Langley and P. F. Taday, *J. Phys. B: At., Mol. Opt. Phys.*, 1999, **31**, L553–L562.
- 56 H. Stapelfeldt and T. Seideman, *Rev. Mod. Phys.*, 2003, **75**, 543–557.
- 57 M. J. J. Vrakking and S. Stolte, *Chem. Phys. Lett.*, 1997, **271**, 209–215.